33RD CONGRESS
OF THE INTERNATIONAL COUNCIL
OF THE AERONAUTICAL SCIENCES
STOCKHOLM, SWEDEN, 4-9 SEPTEMBER, 2022

ICAS 2022 SWEDEN

DESIGN AND STUDY ON NOISE REDUCTION PROPERTIES OF A MULTISTAGE BIONIC MEMBRANE-TYPE ACOUSTIC METAMATERIAL

Zhang Xuanjia[1], Guo Dong[1], Huang Heyuan[1, 2,*]

[1]School of Aeronautics, Northwestern Polytechnical University, Xi'an 710072, China
[2]Aircraft Strength Research Institute, Aviation Industries of China, Xi'an 710069, China
*Corresponding author: Huang Heyuan. E-mail: huangheyuan@nwpu.edu.cn.

Abstract

In order to solve the problem of low frequency noise, a multistage bionic spider web model was designed based on the structural characteristics of spider web. The noise reduction performance of membrane-type acoustic metamaterials based on single stage and plane array of cobweb model is studied by numerical and experimental methods. The results shows that the cobweb model can effectively control the noise propagation. The spider-web model D after planar array has better noise reduction effect compared with spider-web model B and spider-web model C, respectively. By analyzing the intrinsic vibration patterns at the characteristic frequencies near the peak and valley frequencies, it is found that the multi-state anti-resonance mode of the film is the main reason for enhancing the noise reduction of thin-film acoustic metamaterials and widening the noise reduction bandwidth.

Keywords: Biomimetic design; Membrane-type acoustic metamaterials; Low frequency noise reduction

1. introduction

Noise will cause many health problems, so the design and research of noise-reducing acoustic metamaterials is a hot topic at present. Traditional noise-cancelling structures have large mass and poor noise reduction effect [1]. Compared with traditional noise-cancelling materials, thin-film acoustic metamaterials have excellent properties such as small size, light weight and low-frequency noise reduction [2]. Therefore, thin film acoustic metamaterials have a very broad promising in the field of noise reduction [3].

In order to improve the noise reduction performance of the film, Zhou [4] et al designed four acoustic metamaterial models with different resonance distributions, which effectively broadened the acoustic attenuation band in the low-frequency region. Using the same idea, Lu [5] et al. by splitting the ring mass block into four mass blocks, the thin film ring structure can significantly increase the acoustic transmission loss bandwidth of greater than 5 dB by 1325% in the low frequency range of 300 Hz. Yang [6] et al. produced a thin film acoustic metamaterial model with a central mass block attached to an elastic film. Then it was demonstrated through experiments and finite element simulations that the structure produces an acoustic forbidden band in the low frequency range of 200-300 Hz and is capable of achieving complete reflection of the incident low frequency acoustic wave when the frequency of the incident acoustic wave matches the resonant frequency of the structure. However, single-stage thin-film acoustic metamaterials have a narrow STL bandwidth for acoustic transmission loss, a single variable parameter, which limits the noise reduction capability of the structure. How to design the structure of thin-film acoustic metamaterials so as to broaden the low-frequency noise reduction bandwidth remains to be further investigated.

To further investigate the noise reduction characteristics of multi-stage thin-film acoustic metamaterials,

the team of Yang [7] composed a single-layer array of thin-film acoustic metamaterials with thin-film acoustic metamaterials placed with different masses of circular mass blocks on the basis of single-stage thin films. It was demonstrated that the single-layer array of metamaterials could achieve effective acoustic emission of low-frequency noise acoustic waves at multiple frequency points, and an average noise reduction of 40 dB in the low-frequency acoustic wave frequency range of 50 Hz to 1000 Hz could be achieved by a two-layer panel structure of thin-film acoustic metamaterials. In addition, Langfeld [8] proposed a noise reduction structure consisting of two stacked arrangements of thin-film acoustic metamaterials, which can achieve the regulation of the intrinsic vibration shape and acoustic transmission loss of the structure using pressurized air for inflation. Although the multi-stage thin-film acoustic metamaterials designed so far have made some achievements in terms of noise reduction effects. However, most of the current studies on multi-stage thin-film acoustic metamaterials are based on macroscopic phenomenological analysis of the noise reduction effect, while there is no clear explanation of the coupled vibration behavior of thin-film acoustic metamaterials and the coupling characteristics of the structure to the acoustic field, which leads to the inability to precisely control the design parameters of the structure during the design of thin-film acoustic metamaterials [9].

To address the above problems, this paper designs a multi-stage thin-film acoustic metamaterial based on the bionic concept. Then the numerical analysis model of acoustic-solid coupling is established. The correctness of the bionic numerical analysis model is verified by measuring the acoustic transmission loss of the thin film acoustic metamaterial using the four microphone measurement method. The noise reduction amplitude and noise reduction bandwidth are used as the evaluation index of noise reduction performance to determine the best combination of noise reduction performance in the model after the single-stage thin-film planar array. Then, the noise reduction performance of multi-stage thin film acoustic metamaterials is investigated based on the numerical analysis method to clarify the noise reduction mechanism of the bionic thin film acoustic metamaterials.

2. Methodology

2.1 Structural design method

According to the principle of noise reduction and bionics [10, 11], the Single-stage cobweb model is designed as shown in Figure 1(a). The model is formed by bonding pure polyimide (PI) film with ethylene-vinyl acetate copolymer (EVA) square frame, in which the center of PI film is a large cross (“+”) oscillator of EVA material. A staggered small cross and a word (“-”) oscillator are arranged at the end of the large cross. In order to further broaden the noise reduction bandwidth and improve the noise reduction amplitude of thin film acoustic metamaterials, a planar array model is formed for the single-stage square film model array (Figure 1). There are three types of planar array models, the blue oscillator represents the oscillator of EVA material, and the gray represents the oscillator of metal material. The three models are recorded as Model B, Model C, and Model D. The material of the small "-" oscillator of model B is all EVA, the material of the small "-" oscillator on one diagonal of model C is EVA, and the material of the small "-" oscillator of model D is all metal. The schematic diagrams of the three spider web planar array models are shown in Figure 1.

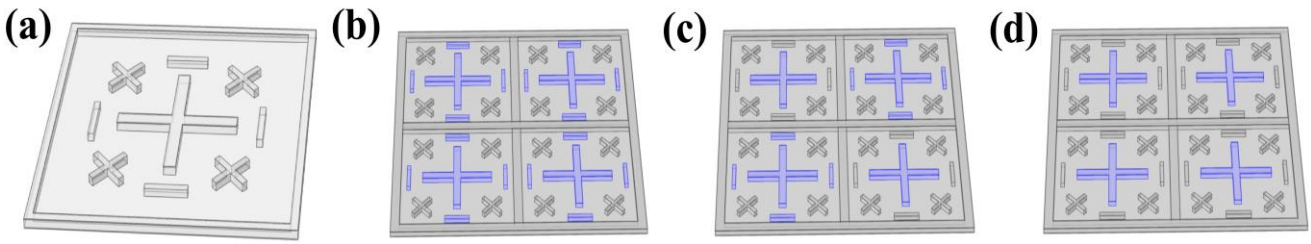

Figure 1 - Schematic diagram of cobweb model: (a) model A; (b) model B; (c) model C; (d) model D

2.2 Experiment and simulation method

The STL of thin film acoustic metamaterials was calculated and analyzed using the acoustic-solid coupling numerical analysis method [5, 12]. As shown in Figure 2(a), the solid mechanics part is first affected by the sound pressure to calculate the frequency response of the diaphragm, which then transmits it to the aeroacoustics domain at the other end, where an analysis is made [12, 13]. The material parameters in the numerical model [14] are shown in Table 1.

Table 1 Thin film acoustic metamaterial parameters

	Young's Modulus (Pa)	Density (kg/m^3)	Poisson's Ratio
PI	1.42 X 10^9	1100	0.36
EVA	1.7 X 10^8	2050	0.45
Metal	2 X 10^{11}	7800	0.33

The sound transmission loss (STL) [15] of the specimen was measured using the four-microphone measurement method (Figure 2(b)). Then, the transmission matrix method is used to calculate the acoustic parameters of the specimen, such as transmission coefficient and acoustic transmission loss [16, 17].

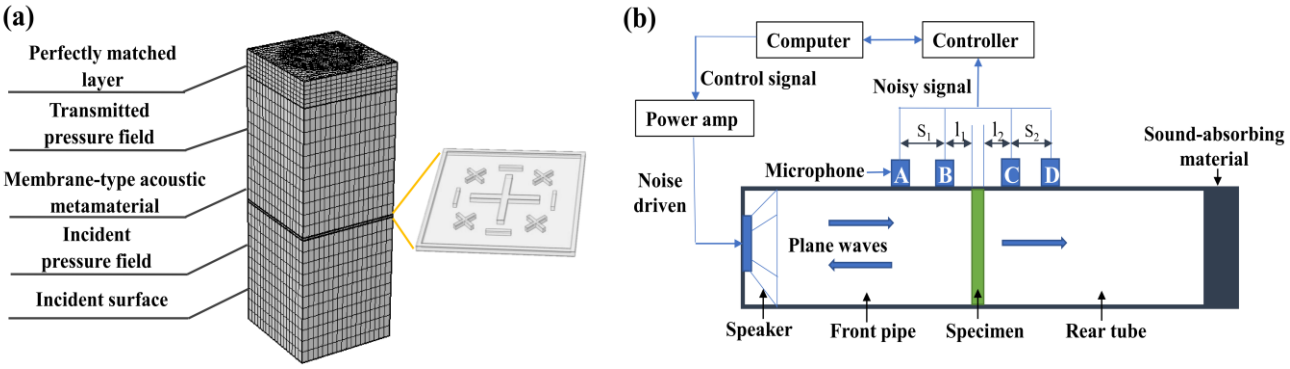

Figure 2 - (a) Film acoustic metamaterial analysis model. (b) Four-microphone method of measurement.

In the experimental and numerical calculations, the band between the first and second valleys in the STL curve is defined as the first STL bandwidth (B_1) The corresponding first and second valley frequencies are defined as the lower (f_1) and upper (f_3) limits of B_1, respectively, and the first peak frequency is defined as f_2. The band between the second and third valleys is defined as the second STL bandwidth (B_2). The corresponding second and third valley frequencies are defined as the lower (f_3) and upper (f_5) limits of B_2, respectively. The second peak frequency is defined as f_4, and the maximum noise reduction is defined as STL_{max}. 25 dB is chosen as the criterion with certain noise reduction effect, and the band width with noise reduction greater than 25 dB in the range of 1600 Hz is defined as B_f. f_1, f_2, f_3, f_4, f_5, B_1, B_2, STL_{max}, and B_f in the above definitions are used as the evaluation of noise reduction performance of all models in this paper metrics.

3. Result and analysis

3.1 Model validation

The overall trend, peak frequency and valley frequency of the STL curve of the single-stage cobweb model A simulation are in well agreement with that of the experiment (Figure 3(a)), which verifies the correctness of the numerical analysis method of acoustic metamaterial of square thin films. The noise reduction performance of multi-stage model D and single-stage spider-web square film model A in the same frequency band is shown in Figure 3(b). Compared with the spider-web square film model A, the peak and valley frequencies of model D are reduced. The noise reduction amplitude of model D is

increased by 9.4% and the noise reduction bandwidth is increased by 2.5% compared to the spider-web square film model A.

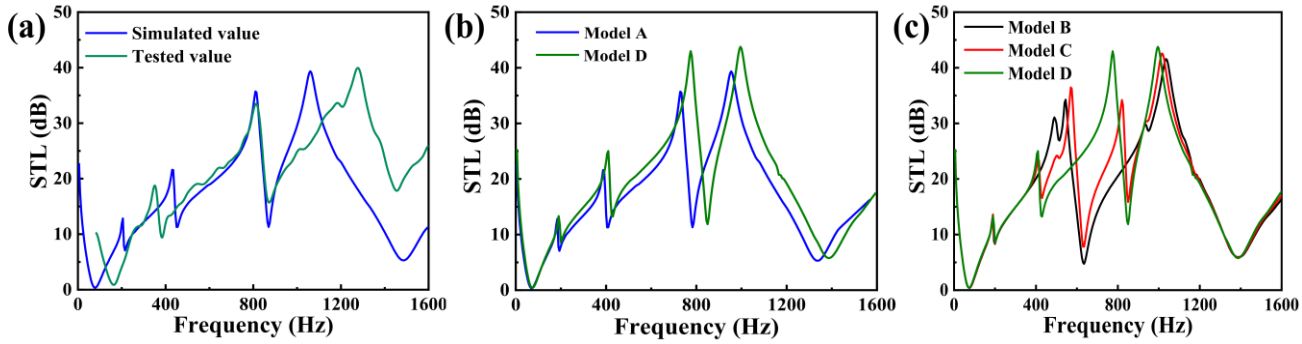

Figure 3 - (a) Comparison of STL curves between simulation and experiment of single-stage square Model A. (b) Comparison of STL curves between Model A and Model D. (c) Comparison of simulated STL curves for three planar array models

Table 2 Comparison of peak and valley frequencies, noise reduction amplitude and bandwidth for the lightweight planar array models

Model	f_1/Hz	f_2/Hz	f_3/Hz	f_4/Hz	f_5/Hz	B_1/Hz	B_2/Hz	STL_{max}/dB	B_f/Hz
Model B	75	545	635	1035	1390	560	755	41.57	400
Model C	75	570	630	1015	1385	555	755	42.58	370
Model D	75	775	850	995	1385	775	535	43.78	410

As can be seen from Figure 3(c) and Table 2, model D has the highest noise reduction amplitude in the 1600 Hz range, with 2.82% more than model B and 5.32% more than model C. Among the three models, the first low-frequency noise reduction bandwidth model D is the widest, with 38.39% more than model B and 39.64% more than model C. The bandwidth model D with noise reduction greater than 25 dB is also the widest, with 2.5% more than model B and 10.81% more than model C. Therefore, the spider web planar array model D has the best noise reduction effect among the three combined models.

3.2 Noise reduction characteristic analysis

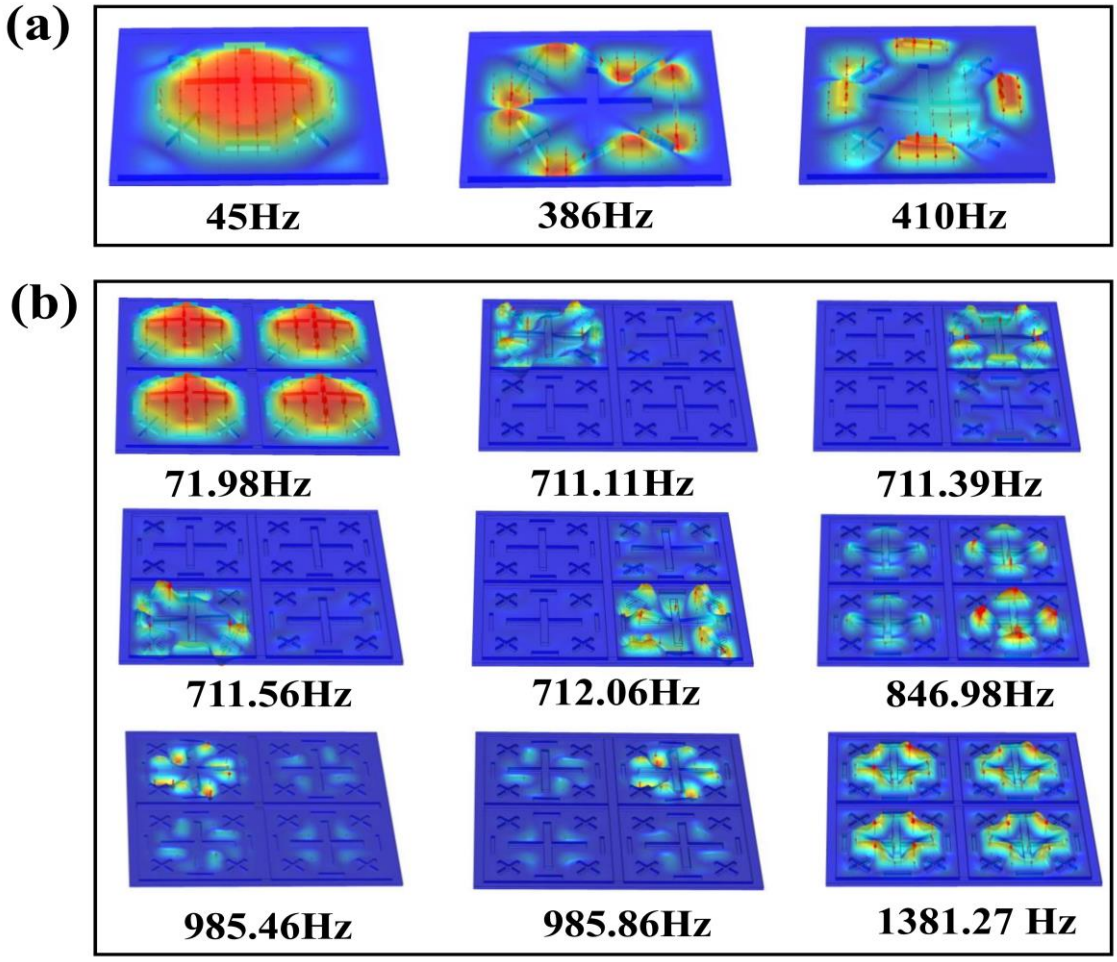

Figure 4 - Cobweb model (a) A and (b) D at characteristic frequencies near peak and valley frequencies.

The intrinsic vibrational modes of model A and model D at the characteristic frequencies near the peak and valley frequencies are shown in Figure 4(a) and 4(b). At the first valley frequency f1, the first-order set total resonance modes occur in all four single-stage models S1, S2, S3, and S4, which are similar to the intrinsic vibration patterns of the spider-web square film model D at f1. At f2, the number of eigenfrequencies of model C is four, corresponding to the four single-stage models, and the values of their eigenfrequencies are basically close to each other, and the inverse resonance modes of small cross oscillators occur in S1, S2, S3, and S4 in turn. At f3, the intrinsic vibration pattern of model C behaves as the resonant mode of the large cross terminal membrane region of the four single-stage models. At f4, model C still appears to have four characteristic frequencies and the values are basically close to each other, S1, S2, S3, and S4 occurring in the anti-resonance mode of the membrane region between the large and small cross oscillators in turn. The intrinsic vibration pattern of model C at f5 shows the resonance mode of the membrane region between the large and small cross oscillators of the four single-stage models.

By analyzing the intrinsic vibration patterns near the peak and valley frequencies of model D, it can be found that the noise reduction valley of the planar array model appears because the four single-stage models co-occur in a local resonance mode. The number of eigenfrequencies near the valley is one. The locations where the local resonance occurs are different at different valley frequencies. The peak frequency of the planar array model is determined by the peak frequency of each single-stage model. The number of eigenfrequencies near the peak is 4, corresponding to each single-stage model. Due to

the coupling effect between the single-stage models, the values of the four eigenfrequencies differ slightly, but are basically close to each other. The planar array model has almost no effect on the intrinsic frequencies of the single-stage model, which are almost the same in peak and valley frequencies as the single-stage model. Compared with the single-stage model, the planar array model does not achieve a further broadening of the noise reduction bandwidth. In addition, the intrinsic oscillations of the planar array model and the single-stage model are basically similar near the peak and valley frequencies, differing only at the peak frequency. The single-stage model works sequentially, meaning that when the anti-resonance mode occurs in one of the single-stage models, the rest of the single-stage models are almost vibration-free, so the noise reduction effect is not much different from that of the single-stage model. In addition the planar array model does not produce more consecutive multi-stage anti-resonance modes, so the overall range of noise reduction is almost unchanged.

4. Conclusion

The results show that the noise reduction of single-stage cobweb model reaches 39.35dB, indicating that the noise reduction effect is obvious. In the combination of spider-web planar array models, spider-web model D has 2.82% and 5.32% more noise reduction amplitude compared with spider-web model B and spider-web model C, respectively. The first noise reduction bandwidth of model D is 38.39% and 39.64% more than that of models B and C, respectively, and the band width of noise reduction greater than 25 dB is 2.5% and 10.81% more than that of model D, respectively, so model D has the best noise reduction effect. In addition, the analysis of the noise reduction mechanism shows that the multi-state antiresonance mode of thin films enables the acoustic metamaterials to have high noise reduction and wide noise reduction bandwidth. The multistage film with planar array has better sound insulation performance at low frequency.

5. Acknowledgments

This work was jointly supported by the General Project of Chongqing Natural Science Foundation (No. cstc2020jcyj-msxmX0784) and China Postdoctoral Science Foundation (2021M693007).

6. Contact Author Email Address

Email: zhangxuanjia@mail.nwpu.edu.cn

7. Copyright Statement

References

[1] Liao G X, Luan C C, Wang Z W, Liu J P, Yao X H and Fu J Z. Acoustic metamaterials: a review of theories, structures, fabrication approaches, and applications. *Advanced Materials Technologies*, Vol. 6, No. 5, 2021.

[2] Zhang X H, Qu Z G and Wang H. Engineering acoustic metamaterials for sound absorption: from uniform to gradient structures. *Iscience*, Vol. 23, No. 5, 2020.

[3] Zhou W J, Wu B, Muhammad, Du Q J, Huang G L, Lu C F and Chen W Q. Actively tunable transverse waves in soft membrane-type acoustic metamaterials. *Journal of Applied Physics*, Vol. 123, No. 16, 2018.

[4] Zhou G J, Wu J H, Lu K, Tian X J, Huang W and Zhu K D. Broadband low-frequency membrane-type acoustic metamaterials with multi-state anti-resonances. *Applied Acoustics*, Vol. 159, 2020.

[5] Lu Z B, Yu X, Lau S K, Khoo B C and Cui F S. Membrane-type acoustic metamaterial with eccentric masses for broadband

sound isolation. *Applied Acoustics*, Vol. 157, 2020.
[6] Yang Z, Mei J, Yang M, Chan N H and Sheng P. Membrane-type acoustic metamaterial with negative dynamic mass. *Physical Review Letters*, Vol. 101, No. 20, 2008.
[7] Yang Z, Dai H M, Chan N H, Ma G C and Sheng P. Acoustic metamaterial panels for sound attenuation in the 50-1000 Hz regime. *Applied Physics Letters*, Vol. 96, No. 4, 2010.
[8] Langfeldt F, Riecken J, Gleine W and Estorff O. A membrane-type acoustic metamaterial with adjustable acoustic properties. *Journal of Sound and Vibration*, Vol. 373, pp 1-18, 2016.
[9] Liu J Y, Guo H B and Wang T. A review of acoustic metamaterials and phononic crystals. *Crystals*, Vol. 10, No. 4, 2020.
[10] Koniczek M, Antonuk L E, El-Mohri Y, Liang A K and Zhao Q H. Theoretical investigation of the noise performance of active pixel imaging arrays based on polycrystalline silicon thin film transistors. *Medical Physics*, Vol. 44, No. 7, pp 3491-3503, 2017.
[11] Sepehri S, Jafari H, Mashhadi M M, Yazdi M R H and Fakhrabadi M M S. Study of tunable locally resonant metamaterials: effects of spider-web and snowflake hierarchies. *International Journal of Solids and Structures*, Vol. 204, pp 81-95, 2020.
[12] Gao N S, Wu J H, Hou H and Yu L. Excellent low-frequency sound absorption of radial membrane acoustic metamaterial. *International Journal of Modern Physics B*, Vol. 31, No. 3, 2017.
[13] Li Z C, Chen S Z, Wu Z C and Yang L. An improved approach for normal-incidence sound transmission loss measurement using a four-microphone impedance tube. *Journal of Vibration and Control*, Vol. 27, No. 3-4, pp 332-342, 2021.
[14] Huang H Y, Cao E R, Zhao M Y, Alamri S and Li B. Spider web-inspired lightweight membrane-type acoustic metamaterials for broadband low-frequency sound isolation. *Polymers*, Vol. 13, No. 7, 2021.
[15] Parrinello A and Ghiringhelli G L. Evaluation of damping loss factor of flat laminates by sound transmission. *Journal of Sound and Vibration*, Vol. 424, pp 112-119, 2018.
[16] Naify C J, Chang C M, McKnight G and Nutt S. Transmission loss of membrane-type acoustic metamaterials with coaxial ring masses. *Journal of Applied Physics*, Vol. 110, No. 12, 2011.
[17] Naify C J, Chang C M, McKnight G, Scheulen F and Nutt S. Membrane-type metamaterials: transmission loss of multi-celled arrays. *Journal of Applied Physics*, Vol. 109, No. 10, 2011.